Redox and Acid−Base Coupling in Ultrathin Polyelectrolyte Films

Mario Tagliazucchi,[†] Ernesto J. Calvo,*[,†] and Igal Szleifer*[,‡]

Molecular Electrochemistry Group, INQUIMAE, DQIAyQF, Facultad de Ciencias Exactas y Naturales, Universidad de Buenos Aires, 1428 Buenos Aires, Argentina, and Department of Biomedical Engineering, Northwestern University, 2145 Sheridan Road, Evanston, Illinois 60208

Received September 3, 2007. In Final Form: November 10, 2007

A single layer of poly(allylamine) with a covalently attached osmium pyridine−bipyridine complex adsorbed onto a Au surface modified by mercaptopropanesulfonate has been studied theoretically with a molecular approach and experimentally by cyclic voltammetry. These investigations have been carried out at different pHs and ionic strengths of the electrolyte solution in contact with the redox polyelectrolyte modified electrode. The theory predicts strong coupling between the acid−base and redox equilibria, particularly for low ionic strength, pH close to the pK_a, and high concentration of redox sites. The coupling leads to a decrease in the peak potential at pH values above the apparent pK_a of the weak polyelectrolyte, in good agreement with the experimental pH dependence at 4 mM $NaNO_3$. Theoretical calculations suggest that the inflection point in the peak position versus pH curves can be used to estimate the apparent pK_a of the amino groups in the polymer. Comparison of the apparent pK_a for PAH-Os in the film with that of poly(allylamine) reported in the literature shows that the underlying charged thiol strongly influences charge regulation in the film. A systematic study of the film thickness and the degree of protonation in sulfonate and amino groups for solutions of different pH and ionic strength shows the coupling between the different interactions. It is found that the variation of the film properties has a non-monotonic dependence on bulk pH and salt concentration. For example, the film thickness shows a maximum with electrolyte ionic strength, whose origin is attributed to the balance between electrostatic amino−amino repulsions and amino−sulfonate attractions.

1. Introduction

Chemically modified electrodes are conductive substrates coated with a film of a selected chemical moiety to introduce desired chemical, electrochemical, or optical properties.[1−3] The film can be a monomolecular layer, a multilayer, or a polymeric coating. In an important number of these systems, there is at least one protonable species, and therefore, the properties of the electrode depend on the pH of the solution in contact or adjacent to the electrode. The theoretical description of this type of interface is complicated due to the fact that the acid−base equilibrium can be shifted by changes in the electrode potential and solution conditions, and this in turn is coupled to the molecular organization of the film.

Smith and White presented a model for an electrode coated with a monolayer of molecules bearing weak acid headgroups.[4] The model predicts a maximum in the capacitance−potential curves due to the dissociation of the acid at increasing metal/electrolyte potential difference. This prediction has been validated by cyclic voltammetry[5] and electrochemical impedance spectroscopy (EIS)[6,7] experiments for thiolated electrodes. The Smith and White model has been extended to incorporate effects arising from the discreteness of charge.[8−10]

In the special case where the redox couple itself is pH-dependent, the redox and acid−base sites in the molecule are separated by a few chemical bonds and therefore they are strongly coupled. It is commonplace to analyze these systems in terms of chemical reactions relating species in different protonation and oxidation states, neglecting intermolecular interactions.[11,12] This analysis has been applied to several examples of pH-dependent redox couples in both monolayer[13,14] and multilayer[15,16] films. Naegeli et al. extended the analysis and combined it with the Donnan partition model to study pH-dependent redox couples inmobilized in Nafion films.[17]

A different case is the simultaneous presence of protonable groups and pH-independent redox couples at the surface. For example, the electrochemical response of mixed acid−ferrocene sulfide monolayers has been reported to strongly depend on solution pH.[18] Consider also a film obtained by covalent binding of a soluble redox species with a fraction of the carboxylates or amines in a polymer[19−21] or in a self-assembled monolayer,[22] where unreacted weak acid/basic groups and attached redox centers coexist. The acid−base and redox equilibria in those cases are expected to be coupled through intermolecular

* To whom correspondence should be addressed. E-mail: calvo@qi.fcen.uba.ar (E.J.C.); igalsz@northwestern.edu (I.S.).

[†] Universidad de Buenos Aires.

[‡] Northwestern University.

(1) Murray, R. W. Introduction to Molecularly Designed Electrode Surfaces. In *Molecular Design of Electrode Surfaces*; Murray, R. W., Ed.; John Wiley and Sons, Inc.: New York, 1992.

(2) Murray, R. W. Chemically Modified Electrodes. In *Electroanalytical Chemistry*; Bard, A. J., Ed.; Marcel Dekker: New York, 1984; Vol. 13, p 191.

(3) Murray, R. W. *Acc. Chem. Res.* **1980**, *13*, 135.

(4) Smith, C. P.; White, H. S. *Langmuir* **1993**, *9*, 1.

(5) White, H. S.; Peterson, J. D.; Cui, Q.; Stevenson, K. J. *J. Phys. Chem. B* **1998**, *102*, 2930.

(6) Bryant, M.; Crooks, R. M. *Langmuir* **1993**, *9*, 385.

(7) Burgess, I.; Seivewright, B.; Lennox, R. B. *Langmuir* **2006**, *22*, 4420.

(8) Andreu, R.; Calvente, J. J.; Fawcett, W. R.; Molero, M. *Langmuir* **1997**, *13*, 5189.

(9) Andreu, R.; Fawcett, W. R. *J. Phys. Chem.* **1994**, *98*, 12753.

(10) Fawcett, W. R.; Fedurco, M.; Kováčová, Z. *Langmuir* **1994**, *10*, 2403.

(11) Laviron, E. *J. Electroanal. Chem.* **1980**, *112*, 1.

(12) Laviron, E. *J. Electroanal. Chem.* **1981**, *124*, 9.

(13) Madhiri, N.; Finklea, H. O. *Langmuir* **2006**, *22*, 10643.

(14) Katz, E. Y.; Shkuropatov, A. Y.; Vagabova, O. I.; Shuvalov, V. A. *J. Electroanal. Chem.* **1989**, *260*.

(15) Takada, K.; Gopalan, P.; Ober, C. K.; Abruña, H. D. *Chem. Mater.* **2001**, *13*, 2928.

(16) O'Connell, K. M.; Waldner, E.; Roullier, L.; Laviron, E. *J. Electroanal. Chem.* **1984**, *162*, 77.

(17) Naegeli, R.; Redepenning, J.; Anson, F. C. *J. Phys. Chem.* **1986**, *90*, 6227.

(18) Beulen, M. W. J.; Van Veggel, F. C. J. M.; Reinhoudt, D. N. *Chem. Commun.* **1999**, *19*, 503.

(19) Danilowicz, C.; Corton, E.; Battaglini, F. *J. Electroanal. Chem.* **1998**, *445*, 89.

(20) Calvo, E. J.; Etchenique, R.; Danilowicz, C.; Diaz, L. *Anal. Chem.* **1996**, *68*, 4186.

(21) Liu, Y.; Zhao, M.; Bergbreiter, D. E.; Crooks, R. M. *J. Am. Chem. Soc.* **1997**, *119*, 8720.

(22) Molinero, V.; Calvo, E. J. *J. Electroanal. Chem.* **1998**, *445*.

10.1021/la702734n CCC: $40.75
Published on Web 02/06/2008

interactions, as we have recently predicted.[23] However, to the best of our knowledge, this coupling has not yet been theoretically described in a systematic way for chemically modified electrodes as a function of the experimentally controlled variables.

In a previous paper,[23] we presented a molecular theory for the description of the structure and equilibrium electrochemical response of ultrathin polymer modified electrodes. The theory explicitly incorporates from a first principle formulation the molecular details of all species in the system, that is, the size, shape, conformation, charge, and charge distribution for each molecular species as well as the different chemical equilibria and the electrostatic, van der Waals, and excluded volume interactions. We applied the theory to a single layer of PAH-Os (a poly(allylamine) partially derivatized with the pH-independent complex $Os(bpy)_2ClPy^{+/2+}$) on a thiolated gold surface. The predictions from the molecular approach were validated by experimental studies, including cyclic voltammetry and ellipsometry. In this paper, we employ the theory to study the coupling between the protonation equilibrium of the amino groups in the polymer and sulfonate groups in the thiol and the redox equilibrium of the osmium redox sites.

2. Theoretical Approach and Molecular Model

A detailed description of the theoretical approach and the molecular model used to describe PAH-Os modified electrodes has been presented elsewhere.[23] The system under consideration comprises a single layer of PAH-Os adsorbed on a thiolated gold electrode schematically shown in Figure 1A. The theory explicitly considers all the different molecular species of the system. They include the salt anions and cations, hydroxyl ions, protons, water, and molecules attached to the surface, namely, mercaptopropanesulfonate (MPS) and the osmium pyridine−bipyridine derivatized poly(allylamine) (PAH-Os). The theory enables the determination of the molecular organization of the film and the inhomogeneous distribution of all the species by functional minimization of the free energy functional of the system. We consider the case in which the film contains a fixed amount of MPS and of adsorbed polymer and it is in contact with a solution characterized by a bulk pH and ionic strength. Thus, the free energy functional is formulated in an ensemble that is grand-canonical for the mobile species and canonical for the attached molecules. In other words, we fix the chemical potential of the cations, anions, hydroxyls, and protons and the total number density of the MPS and the polymers.

The PAH-Os chains are considered by the theory as a combination of a polymer backbone composed of allylamine units and the covalently attached osmium pyridine−bipyridine complexes. The chemical equilibria considered by the theory include the acid−base equilibrium of the amino groups in the polymer backbone and that of the sulfonate groups in the thiol molecules as well as the redox equilibrium between Os(II) and Os(III) in the electroactive centers. Furthermore, the state of each of the chemically active species is assumed to depend on the distance from the surface, due to the inhomogeneous distribution of all the molecular species.

The free energy of the system is written as a functional of the density profile of all the species as well as the probability to find the chain molecules in a given conformation (see ref 23 and the Supporting Information). It contains contributions from the distance-dependent translational entropy of the mobile species, the conformational entropy of the polymer chains, the free energy associated with the different chemical equilibria in the system,

(23) Tagliazucchi, M.; Calvo, E. J.; Szleifer, I. *J. Phys. Chem. C* **2008**, *112*, 458.

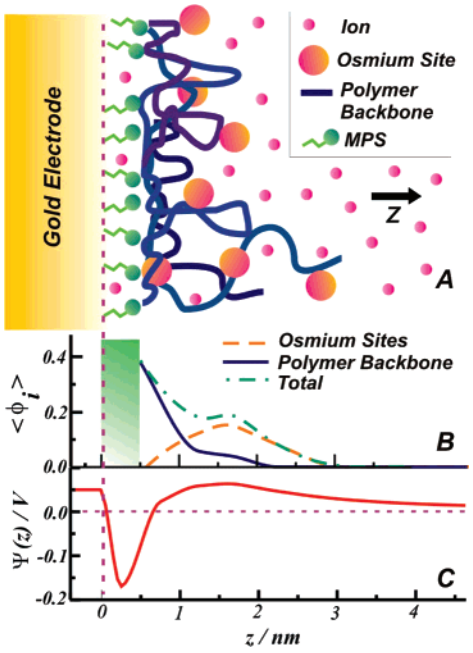

Figure 1. Scheme of the Au/MPS/PAH-Os/solution interface based on the density profiles provided by the theory. The poly(allylamine) backbone and the pyridine−bipyridine osmium complexes of PAH-Os are represented by blue solid lines and big spheres, respectively. The allylamine units in the polymer backbone can be either protonated (charge +1) or deprotonated (neutral). The osmium complexes can be in an oxidized Os(III) (charge +2) state or in a reduced Os(II) (charge +1) state. MPS molecules are covalently assembled to the gold electrode forming a permeable layer. The headgroup in MPS can exist as a negatively charged sulfonate or as a neutral sulfonic acid depending on the local pH. The polymer modified electrode is immersed in an aqueous electrolyte solution containing salt ions, protons, and hydroxyls (depicted as small spheres). The normal direction from the electrode is denoted by z and has its origin on the metal surface. (B) Volume fraction profiles calculated for PAH-Os (dot-dashed line) and its two components: the polymer backbone (full line) and the redox sites (dashed line) calculated for $E = 0.0$ V, $C_{salt} = 0.04$ M, and pH = 7. (C) Electrostatic potential profile calculated for the same conditions as those in (B).

the polymer−polymer and polymer−surface van der Waals (vdW) interaction energies, the electrostatic interaction energies, and the repulsive interactions between all the different molecular species, which are modeled as excluded volume interactions. The minimization of the free energy functional provides for explicit expressions for the distance-dependent densities of the mobile ions, $\rho_i(z)$ (i = w, H^+, OH^-, C, and A for water molecules, protons, hydroxyls, cations, and anions, respectively); the probability distribution function for the polymer, $P_P(\alpha)$; the fraction of charged amino and sulfonate groups, $f_c(z)$ and $f_{c,MPS}(z)$, respectively; the fraction of oxidized redox sites, $f_{Os}(z)$, and the z-dependent electrostatic potential, $\psi(z)$.

The density profiles of the free species, namely, anion, cation, proton, hydroxyl, and solvent, are given by

$$\rho_A(z)\,\upsilon_w = \rho_A^{bulk}\upsilon_w \exp(-\upsilon_A\beta[\pi(z) - \pi^{bulk}] + \beta|e|[\psi(z) - \psi^{bulk}]) \quad (1)$$

$$\rho_C(z)\,\upsilon_w = \rho_C^{bulk}\upsilon_w \exp(-\upsilon_C\beta[\pi(z) - \pi^{bulk}] - \beta|e|[\psi(z) - \psi^{bulk}]) \quad (2)$$

$$\rho_{H^+}(z)\,\upsilon_w = \rho_{H^+}^{bulk}\upsilon_w \exp(-\upsilon_{H^+}\beta[\pi(z) - \pi^{bulk}] - \beta|e|[\psi(z) - \psi^{bulk}]) \quad (3)$$

$$\rho_{OH^-}(z)\,\upsilon_w = \rho_{OH^-}^{bulk}\upsilon_w \exp(-\upsilon_{OH^-}\beta[\pi(z) - \pi^{bulk}] + \beta|e|[\psi(z) - \psi^{bulk}]) \quad (4)$$

$$\rho_w(z)\,\upsilon_w = \rho_w^{bulk}\upsilon_w \exp(-\upsilon_w\beta[\pi(z) - \pi^{bulk}]) \quad (5)$$

where $\beta = 1/k_BT$ is the inverse absolute temperature, $\pi(z)$ is the field coupled to the repulsive interactions and is related to the lateral osmotic pressure,[24] and υ_i is the molecular volume of species i. In eqs 1−5, the distribution of small molecules is seen to depend on the repulsive and electrostatic fields, $\pi(z)$ and $\psi(z)$. As it has been discussed elsewhere, these fields are strongly coupled and depend on the total distribution of molecular species; that is, they are determined by local and nonlocal interactions.[24]

As mentioned above, the theory considers each of the different conformations that the chain molecules can adopt. The minimization of the free energy functional provides for an expression for the probability to find each of those conformations for a given set of conditions. The probability of having a polymer chain in conformation α is given by

$$P_P(\alpha) = \frac{1}{\xi}\exp\{-\int n_P(z,\alpha)[\ln(f_c(z)) + q_{NH_3^+}\beta\,\psi(z)]\,dz + -\int n_{Os}(z,\alpha)[q_{Os(II)}\beta\,\psi(z) + \ln(1 - f_{Os}(z))]\,dz - \beta\,U_{PS}(\alpha) - \int[\upsilon_P(z,\alpha) + \upsilon_{Os}(z,\alpha)][\beta\,\pi(z) + \int\beta\,\chi(|z - z'|)(\langle\phi_P(z')\rangle + \langle\phi_{Os}(z')\rangle)\,dz']\,dz\} \quad (6)$$

where $n_i(z, \alpha)$ and $\upsilon_i(z, \alpha)$ are the number and volume, respectively, of allylamine segments (i = P) or osmium sites (i = Os) that a PAH-Os chain in conformation α has at z, q_i is the charge of group i (i = Os(II) or NH_3^+), $U_{PS}(\alpha)$ is the polymer−surface interaction energy for a chain in conformation α, $\chi(|z - z'|)$ is a distance-dependent vdW interaction parameter, ξ is the normalization constant, and $\langle\phi_i(z)\rangle$ is the average volume fraction of species i at z. The probability of having a chain in a given conformation depends on the state of all the chemical equilibria and on all the interactions, namely, the repulsive and electrostatic interaction fields, $\pi(z)$ and $\psi(z)$, respectively, the polymer−polymer and polymer−surface vdW interactions, and the fraction of oxidized osmium sites and protonated amino groups. Note that, upon changes in the experimentally controlled variables, for example, solution pH, ionic strength, and applied potential on the electrode among others, the interaction fields will change and therefore the probability of the different conformers will change accordingly such that the free energy of the system is minimal.

The theory provides also for the expressions of the generalized acid−base equilibrium constants for the amino groups in the polymer and sulfonate groups in the thiols:

$$K_b^0 = \exp[-\beta\Delta G_c^0] = \frac{\rho_{OH^-}(z)\,f_c(z)}{1 - f_c(z)}\exp(\upsilon_{OH^-}\beta[\pi(z) - \pi^{bulk}]) \quad (7)$$

$$K_{a,MPS}^0 = \exp[-\beta\Delta G_{c,MPS}^0] = \frac{\rho_{H^+}(z)\,f_{c,MPS}(z)}{1 - f_{c,MPS}(z)}\exp(\upsilon_{H^+}\beta[\pi(z) - \pi^{bulk}]) \quad (8)$$

Here, K_b^0 and $K_{a,MPS}^0$ are the thermodynamic equilibrium constants and $\Delta G_{c,MPS}^0 = \mu_{H^+}^0 + \mu_{SO_3^-}^0 - \mu_{HSO_3}^0$ and $\Delta G_c^0 = \mu_{OH^-}^0 + \mu_{NH_3^+}^0 - \mu_{NH_2}^0$ are the thermodynamic Gibbs free energy changes for the reactions:

$$P - NH_2 + H_2O \rightarrow P - NH_3^+ + OH^- \quad (9)$$

$$Au - S(CH_2)_3SO_3H + H_2O \rightarrow Au - S(CH_2)_3SO_3^- + H_3O^+ \quad (10)$$

respectively. P and Au denote the polymer chain and the gold surface, respectively. The thermodynamic equilibrium constants can be multiplied by the constant factor N_A/ρ_w^{bulk} (with N_A being Avogadro's number) to obtain the commonly used equilibrium constants based on molar bulk concentrations, K_a^{MPS} and K_b.[24] In eqs 7 and 8, the thermodynamic equilibrium constants are equal to the product of activities not of concentrations; that is, they explicitly include all the nonideal contributions arising from the intra- and intermolecular interactions, as manifested by the explicit relation between the chemical equilibrium constants and the interactions fields $\pi(z)$ and $\psi(z)$.

In analogy with the generalized acid−base equilibrium equations, the theory provides a generalized Nernst equation for the Os(II)/Os(III) couple:

$$E_{eq}^{abs} = E_{Os(III)/Os(II)}^{0,abs} + \frac{1}{\beta|e|}\ln\left(\frac{f_{Os}(z)}{1 - f_{Os}(z)}\right) + \frac{(q_{ox} - q_{red})}{|e|}(\psi(z) + \lambda) \quad (11)$$

where E_{eq}^{abs} is the electrode potential and $E_{Os(II)/Os(III)}^{0,abs}$ is the standard redox potential for the reaction

$$P - Os(III)^{+2} + e^-(Au) \rightarrow P - Os(II)^+ \quad (12)$$

As was explained in previous work,[23] the electrode potentials in eq 11 are given in the absolute potential scale and can be converted into the experimental potential scale (Ag/AgCl) using the potential of the Ag/AgCl electrode in the absolute scale taken from the work of Trassati.[25,26] In addition, the electrostatic potential at the metal (i.e., $\psi(0)$) differs with the electrode potential in the absolute scale by the work function of the metal.[23,25]

Finally, the variation of the free energy functional with respect to electrostatic potential leads to the Poisson equation

$$\nabla(\epsilon(z)\,\nabla\,\psi(z)) = -\langle\rho_Q(z)\rangle \quad (13)$$

where $\epsilon(z)$ is the position-dependent permittivity and $\langle\rho_Q(z)\rangle$ is the average density of charges at z, given by the sum of the density of charges for all the molecular species. While eq 13 is simple in appearance, the charge distribution in the system is self-consistently determined from the potential of mean force, which is the sum of all the interactions considered by the theory. Since the electrostatic potential is only one contribution to the potential of mean force, eq 13 should be regarded as a generalized Poisson−Boltzmann (PB) equation.

To solve the theory for a given molecular model (the ions and solvent size and shape, the set of conformations for the adsorbed polymer chains, the strength of the molecular interactions, the equilibrium constants and the surface coverages of the thiol molecules and the polymer chains) and experimental condition (pH, ionic strength, electrode potential), we replace eqs 1−12 into the generalized PB equation (eq 13) and the packing constraint equation:

(24) Nap, R.; Gong, P.; Szleifer, I. *J. Polym. Sci., Part B: Polym. Phys.* **2006**, *44*, 2638.

(25) Trasatti, S. *Pure Appl. Chem.* **1986**, *58*, 956.

(26) Trassati, S. *J. Electroanal. Chem.* **1974**, *54*, 19.

$$\sum_i \langle \phi_i(z) \rangle = 1 \quad (14)$$

where $\langle \phi_i(z) \rangle$ is the average volume fraction for species i at z. The nonlinear integro-differential equation system composed by eqs 13 and 14 is then solved using numerical methods. This procedure yields the molecular organization of the film (concentration profile for all species, z-dependent protonation and oxidation fractions, probability distribution function for the polymer chains, and electrostatic potential profile) and the equilibrium electrochemistry. A typical example of the molecular organization predicted by the theory is presented in Figure 1B and C. In Figure 1B, we present density profiles for the polymer and its components, which were used to construct the illustration in Figure 1A. The calculations show that the density of the allylamine segments has a maximum at the thiol−polymer interface due to the strong adsorption forces. On the other hand, the osmium complexes are size-segregated from the electrode surface due to their bulky nature. They also show that while the major part of the polymer is constrained to the first 2 nm from the metal surface, some tails are able to protrude into the solution. These dangling segments tend to adopt extended conformations to minimize the electrostatic repulsions. The electrostatic potential profile is shown in Figure 1C, using the same scale for the z-axis as that in Figure 1A and B to allow for direct comparison. The potential is fixed in the metal region ($z < 0$) and differs from the electrode potential in the Ag/AgCl scale by a constant (see above). A sharp drop is observed in the thiol region ($0 < z <$ 0.5 nm) caused by the negative charges of the sulfonate groups. The potential is then reversed in the polymer region due to the positive charges of the protonated amino and osmium groups. This reversal of the original surface potential is the basis for sequential adsorption of polyelectrolytes in the layer by layer (LbL) method.[27] Finally, the potential tends to zero (its bulk value) for large z. Note that its decay length is determined by the density profile of the dangling tails rather than by the screening of mobile ions (Debye length).

Finally, we will briefly describe the molecular model used in the theory. Molecular volumes and lengths were estimated from molecular models. The thiol molecules were modeled as a layer attached to the gold surface with the reported surface coverage of 4.6×10^{-10} mol/cm^2 (80%)[28] and a thickness of 0.5 nm estimated from the length of thiol molecules. The effective dielectric constant of this layer was calculated to be 3.8 with the Maxwell−Garnet mixing formula[24,29] using 78 and 2 for the dielectric constants of the aqueous solution and organic (thiol) phases, respectively. We allowed mobile ions to penetrate this layer, but not polymer chains. The polymer had a fixed surface density of 2.1 segments/nm^2, which was determined from the Coulombic charge in cyclic voltammograms and the Os/N ratio measured by X-ray photoelectron spectroscopy (XPS).[30] The polymer chains comprised 130 segments and were constrained to have at least one of these segments in contact with the thiol layer to avoid desorption. One segment every 13 had an attached osmium complex, in agreement with the Os/N ratio. The volumes of polymer segments, υ_P, and osmium complexes, υ_{Os}, were 113 and 1770 Å^3, respectively, and the length of the former was 0.5 nm. In a typical calculation, we used a representative sample of 10^5 polymer conformations, which were generated using a modified Rosenbluth−Rosenbluth algorithm as described in ref 23 and in the Supporting Information. The interaction strengths between polymer segments and osmium sites with the thiolated surface were -1.0 kT and -2.0 kT, respectively. Polymer−polymer interactions were chosen to give an effective temperature for the solvent of 0.75θ,[23,31] which is in agreement with the hydrophobicity of the polymeric backbone and the experimental film thickness.[23]

The pK_a values of the previous work have been slightly modified based on new experimental evidence for varying solution pH (see section 4.1). We have modified the pK_a value for the allylamine units from 9.0 to 11.0 (pK_b from 5.0 to 3.0) and the pK_a value for the sulfonate groups in MPS (pK_a^{MPS}) from -1.0 to 0.0. It should be noted that the new value for the pK_a of the allylamine unit is very close to that expected for a primary amine, 10.6.[32] These modifications do not alter the very good agreement between experimental and theoretical electrochemical parameters as a function of salt concentration presented in our previous work (see Figure 1S in the Supporting Information). This result is somehow expected, since the experiments presented in that work were performed at pH 3, and therefore, the PAH-Os was fully protonated for either p$K_a = 9.0$ or p$K_a = 11.0$.

3. Experimental Section

3.1. Reagents and Materials. All solutions were prepared with 18 MΩ Milli-Q (Millipore) water. Sodium 3-mecaptopropanesulfonate (MPS; Aldrich) was used as received. The chemicals employed in electrolyte solutions, $NaNO_3$, HNO_3, and NaOH, were of analytical grade and used without further purification.

The osmium bipyridine derivatized redox polymer $Os(bpy)_2$-$ClPyCH_2NH$−poly(allylamine) (PAH-Os) was synthesized as previously reported.[19] Thiol solutions of 20 mM 3-mercapto-1-propanesulfonic acid (MPS; Aldrich) in 10 mM sulfuric acid (Merck) were prepared before each experiment to avoid oxidation in air. The PAH-Os solution was adjusted to pH 8.3 by employing 0.1 M solutions of HCl or NaOH.

Electrolyte solutions of different pH were obtained by mixing different aliquots of 1 mM NaOH and HNO_3 containing 4 mM $NaNO_3$. The pH of these solutions was measured before and after cyclic voltammetry experiments using a HI 1330 glass electrode (Hanna Instruments). Changes in pH during these experiments were always less than 0.5 units.

3.2. Surface Modification. Silicon (100) substrates were coated with a 200 nm gold layer on a 20 nm titanium and 20 nm palladium adhesion layer by thermal evaporation with an Edwards Auto 306 vacuum coating system at $P < 1 \times 10^{-8}$ bar and employed as electrodes.

The gold film substrates were primed with sulfonate groups by immersion in MPS solution for 30 min and rinsed again with deionized water. The polymer modified electrode was constructed by immersion in PAH-Os solution for 30 min, followed by thoroughly rinsing with Milli-Q water.

3.3. Electrochemical Experiments. Electrochemical experiments were performed using an Autolab PGSTAT 30 potentiostat (Autolab, Ecochemie, Holland) with a purpose built three electrode Teflon cell, with an electrode exposed area of approximately 0.25 cm^2 defined by an inert O-ring. A platinum gauze auxiliary electrode area of large and a Ag/AgCl/3 M KCl (0.210 V versus normal hydrogen electrode (NHE)) reference electrode were employed. All the electrode potentials in this work are expressed in the Ag/AgCl reference potential scale.

Before thiol adsorption, the electrode potential was cycled in 2 M sulfuric acid between 0.2 and 1.6 V at 0.1 V/s to check for surface contamination and electrochemically active areas were calculated from the reduction peak of gold oxide.[33]

(27) Castelnovo, M.; Joanny, J.-F. *Langmuir* **2000**, *16*, 7524.
(28) Mokrani, C.; Fatisson, J.; Guérente, L.; Labbé, P. *Langmuir* **2005**, *21*, 4400.
(29) Croze, O.; Cates, M. *Langmuir* **2005**, *21*, 5627.
(30) Tagliazucchi, M.; Williams, F.; Calvo, E. J. *J. Phys. Chem. B* **2007**, *111*, 8105.
(31) Carignano, M. A.; Szleifer, I. *J. Chem. Phys.* **1994**, *100*, 3210.
(32) *CRC Handbook of Chemical and Physics*, 72nd ed.; Lide, D. R., Ed.; CRC Press: Boston, 1991.

Cyclic voltammograms were recorded at room temperature (25 °C) in the pH range 3−10.5. The liquid junction potentials across the reference electrode frit were estimated using the Henderson equation[34] and used to correct the experimentally measured current potential curves.

A slow scan rate was employed in all electrochemical experiments (0.025 mV/s) to allow for direct comparison with the theoretical predictions valid at equilibrium. We assumed that in those experiments the experimental characteristic time is longer than the characteristic times for charge transfer and diffusional charge transport inside the film, which is confirmed by the almost zero peak separation and constant redox charge observed for cyclic voltammograms measurements at $\upsilon < 0.1$V/s.

4. Results and Discussion

4.1. Electrochemical Response under Reversible Conditions. In our previous work, we showed that the electrochemical response under equilibrium conditions can be calculated from the combination of the redox and non-redox capacitances defined as

$$C_{\text{non-redox}} = \frac{\partial \sigma_M}{\partial E_{eq}^{abs}} \tag{15}$$

$$C_{\text{redox}} = F\frac{\partial \int \langle n_{Os}(z)\rangle f_{Os}(z)\, dz}{\partial E_{eq}^{abs}} \tag{16}$$

Here, F is the Faraday constant and σ_M is the surface charge, equal to $-\epsilon(0)\,(\partial\psi/\partial z)_{z=0}$, where all the quantities in eqs 15 and 16 are readily obtained from the theory. In our previous study, we presented a comparison between experimental and theoretical capacity−potential curves for electrolyte solutions of increasing salt concentration and pH 3, which corresponds to a fully protonated film. We showed that the theory was able to quantitatively reproduce peak positions and peak widths over the entire range of salt concentrations under consideration (0.001−1.2 M). To understand the coupling between acid−base and redox equilibria in the film, here we extend our studies to solutions of different pH. Figure 2A shows the theoretically predicted peak positions as a function of pH for different salt concentrations (Cs). One important result from this figure is that the peak potential is more sensitive to the pH in low salt solutions. We have therefore performed the experiments in 4 mM $NaNO_3$. Figure 2B presents the comparison between theory and experiments, showing that the theory captures the dependence of the peak position on solution pH.

The shift of the voltammetric peak potential from the redox potential of the couple observed in Figure 2 is usually explained in terms of the Donnan interfacial potential.[17,35] This potential arises due to the presence of the electrostatic charges of the polymer excluding ions of same charge from the solution. In the present case, the film bears positively charged amino groups and osmium sites, which shift the voltammetric peak position to positive values with respect to the Os(II)/Os(III) standard redox potential (0.265 V). Figure 2A shows three well-defined regions, which are explicitly indicated. In region I (3 < pH < 10), the number of positive charges in the film is independent of the pH and therefore the peak potential is almost constant. In region II (10 < pH < 12), the deprotonation of the amino groups in the film leads to a decrease of the peak potential at increasing solution pH. Finally, in region III (pH > 12), the major part of the amino groups in the film are deprotonated and therefore the peak position becomes pH-independent again. It is interesting to note that, in region III and at low electrolyte concentration, the peak potential becomes smaller than the potential of the couple (0.265 V). This effect is attributed to the negative charges of the thiol layer. The underlying charged thiol is also responsible for the small shift of the peak position toward higher potentials observed at low pH in Figure 2, which is originated in a decrease in the charge of the thiol due to protonation. The degree of protonation of the sulfonate groups in the thiol will be analyzed in detail in section 4.2.2.

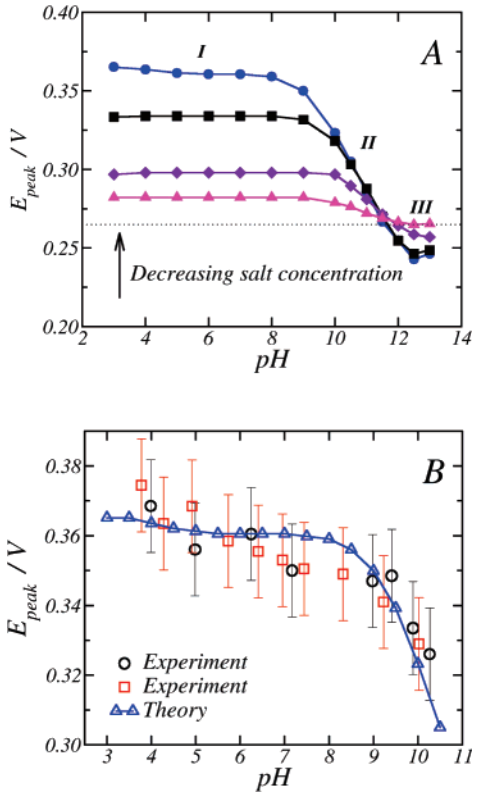

Figure 2. (A) Peak potential position versus solution pH for theoretically determined redox waves for a Au/MPS/PAH-Os electrode immersed in solutions of different added salt concentration. The dotted line indicates the standard potential of the couple in aqueous solution. Cs: 0.004 M (circles), 0.02 M (squares), 0.2 M (diamonds), and 1 M (triangles). (B) Comparison between theoretical and experimental ($\upsilon = 0.025$ V/s) voltammetric peak potentials for electrolyte solutions of different pH (prepared from 1 mM NaOH and HNO_3 solutions containing 4 mM $NaNO_3$). Two different sets of experimental data are presented. The error bars were estimated from three different experiments performed in 1 mM HNO_3 and 4 mM $NaNO_3$.

The shape of the curves in Figure 2A resembles those obtained for pH-dependent redox couples following the $1e^-/1H^+$ mechanism.[15,17] This mechanism involves the exchange of one electron and one proton when the $pK_a^{ox} < pH < pK_a^{red}$ (where pK_a^{ox} and pK_a^{red} are the acid−base constants of the oxidized and the reduced couple, respectively). In analogy to $1e^-/1H^+$ redox couples, it is possible to imagine four different states for the redox film which differ in its oxidation and/or protonation state. Scheme 1 shows the resulting square scheme and explicitly indicates coupled acid−base and redox reactions.

While for pH-dependent couples the peak potential gives information on the pK_a of the redox molecule itself, in the present work, the redox couple acts as a probe reporting on the pK_a of

(33) Finklea, H. O.; Snider, D. A.; Fedyk, J. *Langmuir* **1990**, *6*, 371.
(34) Bard, A. J.; Faulkner, L. R. *Electrochemical Methods: Fundamentals and Applications*, 2nd ed.; John Wiley & Sons: New York, 2001.
(35) Doblhofer, K.; Vorotyntsev, M. Fundamentals. In *Electroactive Polymer Electrochemistry*; Lyons, M. E. G., Ed.; Plenum: New York, 1994; p 375.

Scheme 1. Square Scheme for Au/MPS/PAH-Os Film Showing the Analogy with a $1e^-/1H^+$ Redox System. The Polymeric Backbone Is Denoted by P-.

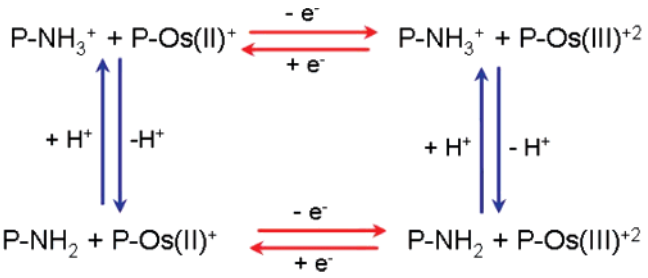

a different chemical species in the film. This effect is not limited to ultrathin layers, since a decrease in the peak potential at increasing pH has also been observed in electrodes modified by PAH-Os and poly(vinyl sulfonate) multilayers.[30]

The choice of pK_a for the amino groups deserves further discussion. The pK_a used in the theory (11.0) was selected to ensure good agreement with experimental observations shown in Figure 2B. This value corresponds to that of an isolated group in the absence of interactions and can therefore be compared with that of a primary amine (10.6). Due to the presence of interactions, the pK_a used in the molecular model could differ with the pH at which half the amino groups are protonated, which will be denoted here as the apparent pK_a^{app}. It is worthwhile to stress that the theory predicts the pK_a^{app} for a given experimental condition, incorporating the effect of molecular interactions (activity coefficients) to the pK_a of the isolated amino groups.

Formally, the pK_a^{app} value is obtained when the average fraction of charged allylamine groups, $\langle f_c \rangle$, is equal to 0.5. Due to the inhomogeneous distribution of allylamine groups and charged groups (see Figure 1), we define the average fraction of charged groups as

$$\langle f_c \rangle = \frac{\int \langle n_p(z) \rangle f_c(z)\, dz}{\int \langle n_p(z) \rangle\, dz} \qquad (17)$$

We can now use the theoretically calculated peak potential versus pH curves to investigate whether electrochemistry could provide a way to estimate the apparent pK_a of the amino groups in the film. It may be appealing to fit the theoretical data to the $1e^-/1H^+$ mechanism.[11,13] While the model fits the curves well, the best fit values for the pK_a of the reduced and oxidized films (11.5 and 9.6 for Cs = 0.004 M) do not agree with those obtained from eq 17 (11.8 and 11.7), showing that the analogy with pH-dependent couples cannot be extended so far. We have found that the inflection point of the curves in Figure 2A provides a simpler and better way to estimate the pK_a^{app}. As an example, the pHs at the inflection point for Cs = 0.004, 0.2, and 1 M are 11.1, 11.2, and 10.8, respectively, which should be compared with the pK_a^{app} values determined from $\langle f_c \rangle = 0.5$, which are 11.8, 11.2, and 11.0, respectively.

4.2. Molecular Organization at the Interface. In the previous section, we analyzed the electrochemical behavior for the Au/MPS/PAH-Os interface in electrolyte solutions of different composition. In the rest of this work, we will study the effect of the solution pH, ionic strength, and electrode potential on the molecular organization at the interface. One of the strengths of using a molecular theory in studying the properties of the modified electrodes is that we obtain structural information (in addition to electrochemical and thermodynamic properties) that is difficult to access by experiment.

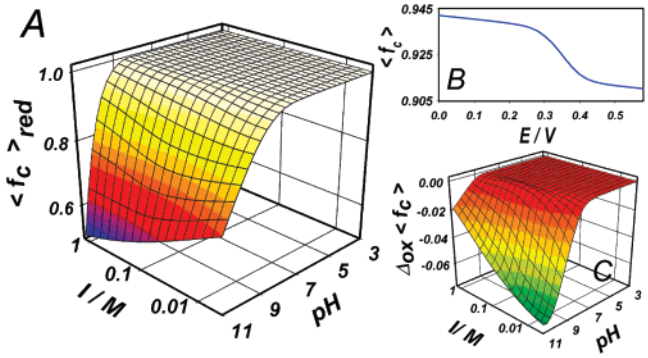

Figure 3. (A) Average fraction of charged amino groups in the polymer (defined by eq 17) for a reduced film (E = 0.0 V) plotted against the pH and ionic strength of the solution. (B) Dependence of the average fraction of charged amino groups on the electrode potential for pH = 9 and I = 0.004 M. (C) Variation in the average fraction of charged amino groups from the fully reduced (E = 0.0 V) to the fully oxidized (E = 0.6 V) state (defined by eq 18) calculated for solutions of different pH and ionic strength.

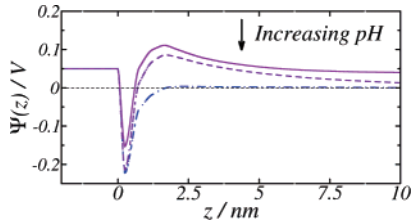

Figure 4. Effect of the solution pH on the electrostatic potential profile: pH = 3 (solid line), 9 (dashed line), and 11.5 (dot-dashed line). The calculations correspond to E = 0.0 V and I = 0.004 M.

4.2.1. Fraction of Protonated Amino Groups in the Polymer. To quantify how the protonation/deprotonation equilibria (eqs 9 and 10), affect the population of electrostatic charges, the average fraction of charged allylamine groups, $\langle f_c \rangle$ (see eq 17), is presented in Figure 3A. As was previously mentioned, a substantial fraction of uncharged amines only exists in basic solutions (pH > 10). The fact that the degree of charging depends not only on the solution pH but also on the ionic strength stresses the importance of chemical equilibria and electrostatic potential coupling. For example, Schlenoff and Rmaile have shown that the internal pK_a in polyelectrolyte multilayers depends on the external salt concentration.[36]

The deprotonation of the polymer layer at high pH has important consequences for the adsorption of a second layer of an oppositely charged polyelectrolyte. As displayed in Figure 4, for a solution pH above the pK_a^{app}, the electrostatic potential profile does not show charge reversal, whereas acidic to weakly basic solutions present this effect. This result can explain why PSS/PAH present irregular growth when assembled at pH = 10.[37]

The degree of protonation in Figure 3A for the fully reduced film (E = 0.0 V) changes during the potential scan to accommodate the newly created Os(III) sites. The evolution of the average fraction of charged amino groups, $\langle f_c \rangle$, with the electrode potential is depicted in Figure 3B. This figure presents a sigmoidal shape, indicative of the charge regulation of the amino groups triggered by Os(II) oxidation. This effect and the shift in peak position (apparent Os(II)/Os(III) redox potential) with the solution pH are the two manifestations of the acid−base and redox coupling.

(36) Rmaile, H. H.; Schlenoff, J. B. *Langmuir* **2002**, *18*, 8263.
(37) Smith, R. N.; McCormick, M.; Barrett, C. J.; Reven, L.; Spiess, H. W. *Macromolecules* **2004**, *37*, 4830.

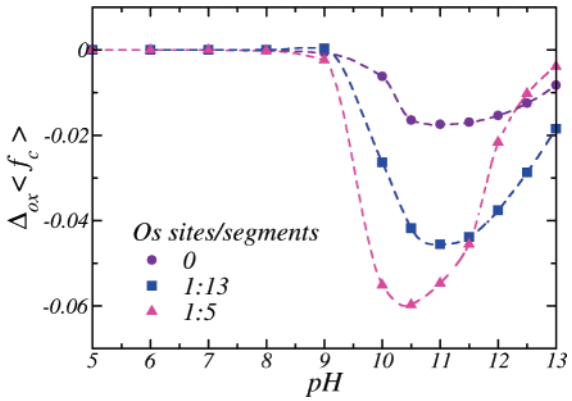

Figure 5. Change in the average fraction of protonated amino groups when the electrode potential increases from $E = 0.0$ V to $E = 0.6$ V as a function of solution pH for PAH-Os chains with different fractions of osmium sites to polymer segments. Calculations were performed at $I = 0.12$ M.

The extent of the redox driven deprotonation can be analyzed by defining the variation of the average charged fraction upon oxidation, $\Delta_{ox}\langle f_c\rangle$ as

$$\Delta_{ox}\langle f_c\rangle = \langle f_c\rangle(E = 0.6\text{ V}) - \langle f_c\rangle\,(E = 0.0\text{ V}) \qquad (18)$$

Figure 3C shows the dependence of $\Delta_{ox}\langle f_c\rangle$ on the electrolyte composition and bulk pH. The coupling between the acid−base and redox equilibria is only efficient under particular conditions that are high pH and low salt concentration. The latter condition is imposed by the fact that in high salt solutions counterion uptake is the predominant charge compensation mechanism. The condition on the solution pH requires a deeper analysis. A plot of the pH-dependence of $\Delta_{ox}\langle f_c\rangle$ is presented in Figure 5 for an extended pH region and different ratios of osmium sites to allylamine units. Specifically, we present results for three different polymer coatings, where the difference between the polymers is the fraction of functional osmium (redox) groups. In the particular case where the Os sites to polymer segments ratio is 0, the film is composed by the non-redox polyelectrolyte poly(allylamine) (PAH). It is clear from this figure that charge compensation by protonation is favored when the solution pH is close to the apparent pK_a. To gain further insight on this result, let us combine eqs 7 and 4 and solve for the fraction of charged groups. After rewriting in terms of proton molar concentration and the K_a of amino groups,

$$f_c(z) = \frac{1}{1 + \dfrac{K_a}{[H^+]}\exp(\beta|e|\,\psi(z))} \qquad (19)$$

The limit of eq 19 when $[H^+] \gg K_a$ or $[H^+] \ll K_a$ is 1 or 0, respectively. Only in the case where $[H^+] \approx K_a$, the increase in $\psi(z)$ that occurs during film oxidation can effectively lead to a variation in $f_c(z)$. Note that, in eq 19, the higher the electrostatic potential, the smaller the fraction of protonated groups.

Figure 5 shows that some deprotonation during potential excursion occurs even for the non-redox film, driven by the effect of the electrode potential on the local electrostatic potential in the polymer region. The magnitude of the effect shows a large increase upon the introduction of osmium sites, showing the presence of a coupling between acid−base and redox equilibria. The figure shows that this coupling can be incremented by increasing the osmium content, and therefore, the maximum effect of ∼7% deprotonation presented in Figure 3C can be further

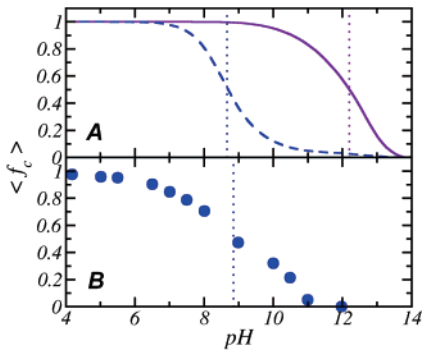

Figure 6. (A) Calculated average degree of protonation for PAH films adsorbed on neutral (dashed line) and thiolated negatively charged (solid line) surfaces (Cs = 0.001 M). (B) Experimental protonation degree for the amino groups in a PAH cast film taken from ref 39. The apparent pK_a's are indicated with dotted lines.

incremented by increasing the polymer degree of derivatization. While in Figure 5 the range of pH limits the minimum ionic strength to 0.1 M, calculations performed at lower ionic strength (not shown) demonstrated that $\Delta_{ox}\langle f_c\rangle$ is limited by the ratio of redox groups to allylamine segments. This result can be rationalized by considering that the amino groups become deprotonated as a result of the creation of new positive charges due to osmium oxidation, and thus, the number of expelled protons should be always smaller than the number of newly created charges. Several functional properties of ultrathin polymeric films are governed by the solution pH. Examples include ionic permeability,[21] wettability, surface friction,[38] and light absorption by pH-dependent probe molecules.[36] Based on our results, we envision that the coupling between acid−base and redox equilibria could be used to turn pH-responsive properties into a redox response by including redox active moeties.

In the previous section, we mentioned that the pK_a^{app} of the amines in the film is close to 11. This result is somehow unexpected, since several authors reported that the apparent pK_a of PAH in aqueous solution and in solution cast films lies in the range 8−9.[39] To explain this apparent contradiction, in Figure 6, we present a comparison of the experimental degree of protonation for a PAH film cast on ZnSe measured by Choi and Rubner[39] with the corresponding values predicted with the molecular theory, $\langle f_c\rangle$, for (i) a PAH layer (without osmium sites) adsorbed over a noncharged surface and (ii) a PAH layer over the MPS modified electrode (both at Cs = 1 mM). This figure shows that the theory only predicts a pK_a^{app} value similar to the reported value when the substrate is uncharged, as it is in the experimental system.[39] For the thiolated surface, the whole titration curve is shifted to higher pH. In this case, the negative charges on the thiol induce the protonation of the amine groups, increasing their pK_a^{app}. The same effect has also been observed in multilayer films, where the pK_a^{app} of embedded weak polyelectrolytes is affected by the presence of the oppositely charged polyions.[39]

In the system under study, the thiol and polymer are located in different regions (see Figure 1A). In a theoretical study of the surface Donnan effect, Ohshima and Ohki have shown that the electrostatic potential inside a membrane (Donnan potential) is only affected by the charge at the interfaces when the membrane thickness is smaller than $1/\kappa_{DH}$ (κ_{DH} is the Debye−Huckel parameter).[40] The strong influence of the charges in the thiol on the pK_a^{app} of the amino groups is therefore only possible because

(38) Burke, S. E.; Barrett, C. J. *Biomacromolecules* **2003**, *4*, 1773.
(39) Choi, J.; Rubner, M. F. *Macromolecules* **2005**, *38*, 116.
(40) Ohshima, H.; Ohki, S. *Biophys. J.* **1985**, *47*, 673.

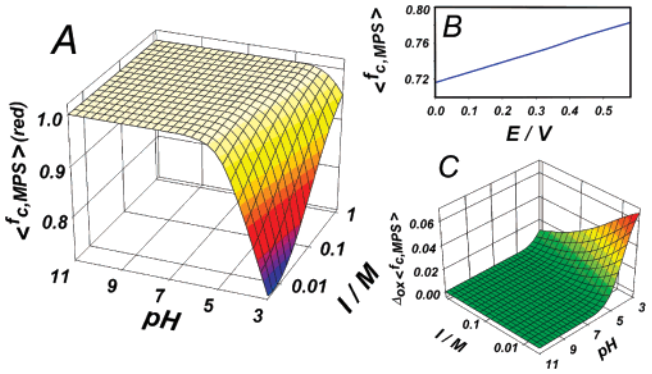

Figure 7. Same plots as Figure 3 for the fraction of charged MPS molecules (part B was calculated for pH = 3 and I = 0.004 M).

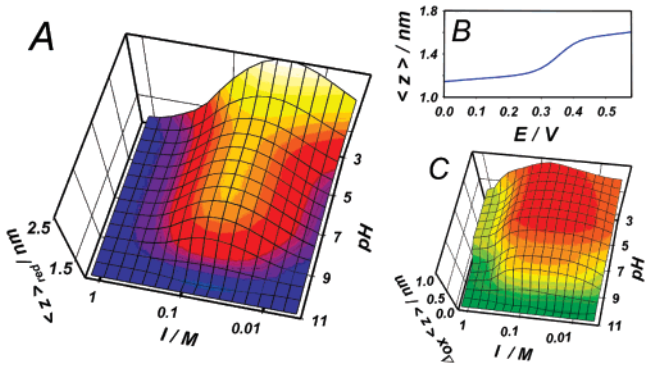

Figure 8. (A) Dependence of the theoretical film thickness in the reduced state (E = 0.0 V) on the pH and ionic strength of the outer electrolyte solution. (B) Theoretical thickness as a function of the electrode potential for pH = 7 and I = 0.004 M. (C) Variation in film thickness from the fully reduced (E = 0.0 V) to the fully oxidized (E = 0.6 V) state (defined by eq 22) as a function of the pH and ionic strength of the electrolyte solution.

the decay length of the electrostatic potential is larger than the thickness of the film.

4.2.2. Fraction of Charged Sulfonate Groups in the Thiol. The degree of charging of a self-assembled monolayer is relevant for its surface properties. Several techniques have been applied to characterize the acid−base behavior of these films, including contact angle,[41] atomic force microscopy (AFM),[42] Fourier transform infrared spectroscopy (FTIR),[43] indirect laser-induced temperature jump (ILIT),[44] and second harmonic generation (SHG) measurements.[45]

In Figure 7A, we show the average degree of charging of the underlying MPS molecules, $\langle f_{c,MPS}\rangle$ (defined from $f_{c,MPS}(z)$ in analogy with $\langle f_c\rangle$; see eq 17), as a function of solution pH and ionic strength. Even though sulfonate groups are strong acids (we have used $pK_a = 0$), thiol protonation is observed at pH < 4 due to the effect of the electrostatic interaction in the local activity of these groups.[46]

The fraction of charged sulfonate groups in the thiol shows a small dependence on the electrode potential, as depicted in Figure 7B. In this case, the relationship is linear instead of sigmoidal. Thiol deprotonation during a potential scan is therefore related to the electrostatic potential at the metal rather than to the fraction of oxidized osmium sites. Changes in the fraction of sulfonate protonation can be studied with the variation of the average charged fraction upon oxidation, $\Delta_{ox}\langle f_{c,MPS}\rangle$, defined in analogy to eq 18, as

$$\Delta_{ox}\langle f_{c,MPS}\rangle = \langle f_{c,MPS}\rangle\,(E = 0.6\text{ V}) - \langle f_{c,MPS}\rangle\,(E = 0.0\text{ V}) \tag{20}$$

We present a plot for $\Delta_{ox}\langle f_{c,MPS}\rangle$ calculated for different electrolyte compositions in Figure 7C. The coupling between the electrostatic potential at the metal and acid−base equilibria is favored again at low ionic strength and pH close to the apparent pK_a. Previous theoretical studies for protonable self-assembled monolayers[4,5] have shown that film protonation/deprotonation gives raise to a peak in the capacitance as a function of the electrode potential near the pK_a of the thiol. This effect is not observed in our case due to the high acidity of the sulfonate groups ($pK_a^{MPS} = 0$) and the presence of a large redox capacitance.

4.2.3. Film Thickness. The polymer chain can preferentially adopt an extended or a collapsed conformation depending on the interplay of intramolecular and intermolecular forces, which is ultimately determined by the experimental conditions. We showed that the probability distribution function for the conformations of the polymer (eq 6) has contributions from all the interactions as well as the different chemical equilibria considered by the theory. Thus, the structure of the polymer layer will be the result of those interactions and chemical equilibria, resulting in the type of detailed density profiles presented in Figure 1. The changes in the structural properties of the polymer layer can be studied by looking at the average film thickness as a function of the different variables. We define this quantity as the first moment of the polymer density distribution, namely

$$\langle z\rangle = \frac{\int(\langle\phi_P(z)\rangle + \langle\phi_{Os}(z)\rangle)(z - \delta_{MPS})\,dz}{\int(\langle\phi_P(z)\rangle + \langle\phi_{Os}(z)\rangle)\,dz} \tag{21}$$

This quantity represents a weighted average of the detailed distributions shown in Figure 1 and is a more concise quantity for the systematic study of changes in the structure of the layer with the experimentally controlled variables.

The effect of the solution conditions, both the pH and ionic strength, on $\langle z\rangle$ is shown for a reduced film (E = 0.0 V) in Figure 8A. In acidic and neutral solutions, film thickness is a non-monotonic function of the ionic strength. The maximum observed at $I \sim 0.05$ M originates from the delicate balance that exists between electrostatic polymer−polymer repulsions and polymer−thiol attractions, which favor extended and collapse conformations, respectively. At $I > 0.1$ M, the electrostatic charges in the film are screened by mobile ions producing a collapsed film. Swelling occurs in the range 0.01 M < I < 0.1 M driven by the electrostatic repulsions between positive charges in the film. An inspection of the polymer density profiles reveals that, during film swelling, there is a marked increase in the population of dangling tails. In low salt solutions (I < 0.01 M), mobile ions not only fail to screen the repulsions between positive charges in the film but also fail to screen the attraction of PAH-Os positive charges to negative charges in the thiol, leading to film contraction. This explanation is supported by calculations performed for a PAH film over a noncharged substrate and in a pH 3 solution, which show a monotonically decreasing thickness with ionic strength. A similar mechanism has been proposed for the adsorption of a strong polyelectrolyte on a oppositely charged

(41) Bain, C. D.; Whitesides, G. M. *Langmuir* **1989**, *5*, 1370.
(42) Hu, K.; Bard, A. J. *Langmuir* **1997**, *13*, 5114.
(43) Sun, L.; Crooks, R. M.; Ricco, A. J. *Langmuir* **1993**, *9*, 1775.
(44) Smalley, J. F.; Chalfant, K.; Feldberg, S. W.; Nahir, T. M.; Bowden, E. F. *J. Phys. Chem. B* **1999**, *103*, 1676.
(45) Konek, C. T.; Musorrafiti, M. J.; Al-Abadleh, H. A.; Bertin, P. A.; Nguyen, S. T.; Geiger, F. M. *J. Am. Chem. Soc.* **2004**, *126*, 11754.
(46) Ninham, B. W.; Parsegian, V. A. *J. Theor. Biol.* **1971**, *31*, 405.

surface,[47] which presents in some cases a maximum in the amount of adsorbed polymer as a function of the ionic strength.

It is interesting to note that a non-monotonic dependence of film thickness on ionic strength has also been experimentally observed and theoretically predicted for poly(acrylic) (PAA) brushes.[48−51] For both PAA brushes and PAH-Os adsorbed on MPS, the screening of polymer charges by mobile ions is responsible for film contraction in high salt solutions. On the other hand, the physical reason for the decrease in film thickness at low ionic strength is different for both systems. In the case of PAA brushes, this effect results from changes in the degree of protonation with the ionic strength. In other words, a decrease in salt concentration induces the reduction of the polymer charge (protonation) to minimize electrostatic repulsions (i.e., charge regulation), and this decrease in the Coulombic repulsions leads to film collapse. This mechanism does not explain the maximum observed in acidic and neutral solutions for PAH-Os adsorbed on MPS because, as was shown in Figure 3A, poly(allylamine) chains remain fully charged up to pH ∼ 9. Therefore, we conclude that, up to pH 9, the non-monotonic behavior of film thickness for PAH-Os is mainly due to thiol−polymer electrostatic interactions. In basic solutions (pH > 9), the PAH-Os film collapses independently of solution ionic strength, since as the charge on the amino groups decreases due to deprotonation, the film contracts due to polymer−polymer and polymer−surface vdW interactions.

Figure 8B shows the dependence of film thickness on the potential applied to the electrode. The shape of the thickness−potential curve resembles that of the fraction of oxidized species versus electrode potential curve, suggesting that the increase in film thickness has an origin in the oxidation of osmium sites. The same behavior has been experimentally observed for PAH-Os/glucose oxidase[52] and PAH-Os/poly(vinyl sulfonate) multilayers.[53] To study the effect of the electrolyte composition, we define the increase in film thickness upon oxidation, $\Delta_{ox}\langle z\rangle$, as the difference in film thickness between the fully oxidized and fully reduced films:

$$\Delta_{ox}\langle z\rangle = \langle z\rangle\,(E = 0.6\ \text{V}) - \langle z\rangle\,(E = 0.0\ \text{V}) \qquad (22)$$

Figure 8C shows a plot of $\Delta_{ox}\langle z\rangle$ as a function of ionic strength and pH. It can be observed that the redox driven swelling is maximum for $I \sim 0.05$ M. Comparison with Figure 8A shows that under those conditions film thickness is strongly dependent on the balance of the different electrostatic interactions in the film, and therefore, a small increase in the fraction of oxidized sites leads to a higher degree of swelling.

5. Conclusions

We have extended our previous theoretical and experimental study of a single layer of PAH-Os adsorbed on a thiolated surface to investigate the effect of ionic strength and solution pH on electrochemical behavior and molecular organization. The molecular theory has allowed us to characterize the connection between film structure, chemical equilibria, and intermolecular forces. In particular, we have focused our attention on the coupling between acid−base and redox equilibria. The coupling is stronger in low salt solutions, showing that its nature is mainly electrostatic. It is also promoted by those experimental conditions where the redox and acid−base equilibra are more easily displaced, namely, pH close to the pK_a^{app} and E close to the peak potential, respectively.

The two manifestations of the acid−base and redox coupling are the decrease of the peak potential at higher solution pH and the deprotonation of amino groups during film oxidation. We have presented experimental evidence in agreement with the first effect, whereas redox driven deprotonation was not experimentally proved. To measure the latter effect, an experimental technique able to measure *in situ* the ionization degree of the protonable groups is needed. This requirement can be fulfilled for polyelectrolytes bearing carboxylic acid groups using IR spectroscopy. We expect this effect to be experimentally verified in the future.

The underlying thiol strongly affects the apparent pK_a of the amino groups in the film and is responsible for some minor features observed in the pH dependence of the peak potential. These effects demonstrate the importance of the charge on the interfaces, which is a direct consequence of the extremely small thickness of the film ($d \sim 1-2$ nm). The interfacial charges are neglected in the Donnan partition model, and therefore, it cannot be used to analyze ultrathin layers. In addition, the Donnan model neglects the distribution of polymer chains across the interface which, as predicted in the present work (see Figure 1), is highly inhomogeneous.

The molecular organization of the polymer film was studied in terms of the detailed density profile and in a systematic way through the first moment of the distribution, that is, the average film thickness. We have shown that the coupling between the molecular interactions and the chemical equilibria is dependent on the solution pH and ionic strength. This effect manifests itself in a non-monotonic variation of the film thickness with ionic strength. The presence of a maximum in the polymer layer height with ionic strength reveals a nontrivial balance between the different intermolecular interactions that can be tuned by the bulk pH. The understanding of the manipulation of the electrochemical and structural properties of the film on experimentally controllable variables can be used in the design of electrode modifiers with desired properties.

Acknowledgment. E.J.C. and M.T. acknowledge financial support from CONICET (Argentina), the University of Buenos Aires, and ANPCyT (BID 1728 OC-AR PICT 2003 No. 06-17170). M.T. has a cooperative CONICET-FUDETEC industrial research grant. E.J.C. is a permanent research staff of CONICET. I.S. acknowledges financial support from the National Science Foundation of the United States CTS-0338377 and NIRT-0403903 and the Raices-Milstein Program of the Argentine Secretary for Science and Technology (SETPCyT).

Supporting Information Available: Complete expression of the free energy functional of the system, description of the chain model and generation, glossary, and comparison of theoretically and experimental peak positions and widths for different ionic strengths and pH 3. This material is available free of charge via the Internet at http://pubs.acs.org.

LA702734N

(47) van de Steeg, H. G. M.; Cohen Stuart, M. A.; de Keizer, A.; Bijsterbosch, B. H. *Langmuir* **1992**, *8*, 2538.
(48) Israëls, R.; Leermakers, F.; Fleer, G. J.; Zhulina, E. B. *Macromolecules* **1994**, *27*, 3249.
(49) Wu, T.; Gong, P.; Szleifer, I.; Vlček, P.; Šubr, V.; Genzer, J. *Macromolecules* **2007**, *40*, 8756.
(50) Gong, P.; Wu, T.; Genzer, J.; Szleifer, I. *Macromolecules* **2007**, *40*, 8765.
(51) Wu, T.; Genzer, J.; Gong, P.; Szleifer, I.; Vlček, P.; Šubr, V. Behavior of surface-anchored poly(acrylic acid) brushes with grafting density gradients on solid substrates In *Polymer Brushes*; Brittain, B., Advincula, R., Caster, K., Eds.; Wiley & Sons, 2004; p 287.
(52) Forzani, E. S.; Pérez, M. A.; Teijelo, M. L.; Calvo, E. J. *Langmuir* **2002**, *18*, 9867.
(53) Tagliazucchi, M.; Grumelli, D.; Bonazzola, C.; Calvo, E. J. *J. Nanosci. Nanotechnol.* **2006**, *6*, 1731.